Accpted for publication in:
2018 International Power Electronics Conference
DOI: 10.23919/IPEC.2018.8508009

Operation of a Modular Multilevel Converter Controlled as a Virtual Synchronous Machine

Salvatore D'Arco[1*], Giuseppe Guidi[1], and Jon Are Suul[1,2]
[1]SINTEF Energy Research, Trondheim, Norway
[2]Department of Engineering Cybernetics, Norwegian University of Science and Technology, Trondheim, Norway
E-mail: salvatore.darco@sintef.no, Giuseppe.Guidi@sintef.no, Jon.A.Suul@sintef.no

***Abstract*-This paper presents an implementation of a Virtual Synchronous Machine (VSM) based on a Modular Multilevel Converter (MMC). The control system relies on the internal simulation of an electromechanical swing equation, which emulates the inertia and damping effect of a synchronous machine and provides the frequency and phase angle needed for controlling the MMC to operate as a VSM. The ac-side control is based on cascaded voltage and current controllers in a synchronous reference frame defined by the virtual swing equation. The reference signals for the ac-side voltage control are generated from a reactive power control loop and a quasi-stationary virtual impedance which emulates the equivalent voltage drop over the stator windings of a synchronous machine. The control system also includes internal control loops for regulating the double frequency circulating currents of the MMC. The presented VSM implementation is tested in a laboratory environment using an MMC with 18 half-bridge sub-modules per arm. Experimental results demonstrate the operation of the VSM-controlled MMC when connected to an external ac grid and in islanded mode feeding a resistive load.**

Keywords— HVDC Transmission, Modular Multilevel Converter, Virtual Inertia, Virtual Synchronous Machine

I. INTRODUCTION

The concept of Virtual Synchronous Machines (VSM), as first introduced in [1], allows for controlling power electronic converters so that they emulate the general characteristics of synchronous generators. This approach for control system design has been motivated by the expected decreasing equivalent inertia of power systems resulting from large-scale integration of distributed generation systems with power electronic grid interfaces and the corresponding decommissioning of traditional thermal power plants with synchronous generators [2]. Thus, the main purpose of VSM based control strategies for power electronic converters is to emulate the inertia and the damping of synchronous machines (SMs) [3].

Emulation of SM characteristics can be achieved by introducing an internal simulation of a virtual swing equation as part of the control system of a power electronic converter [1], [3]-[6]. In this case, the speed and phase angle of the virtual swing equation should be explicitly represented as state variables in the simulation, and the control system should rely on a power-balance-based synchronization mechanism in the same way as a SM. Such approaches for SM emulation will ensure that the control system will be suitable for grid connected operation as well as islanding of systems dominated by power electronic converters [1], [3], [4] [7]. Alternatively, the power provided by a converter with a conventional control system could be controlled to emulate the inertial characteristics of a traditional generator [2], [8], [9]. However, this approach must rely on measurement of the grid frequency and its derivative, usually by a Phase Locked Loop, which implies that the control strategy is not suitable for islanded operation [3].

Since power system operation with very low equivalent physical inertia is already becoming a reality in microgrids or small islanded power systems, such applications have been studied already with the first concepts for VSM-based control that was introduced in the literature [1], [10], [11]. However, the expected future challenges of operating large-scale interconnected power systems with low inertia are already emerging [12], [13]. In this context, HVDC converter stations might be especially relevant for implementation of control strategies for providing virtual inertia, due to the high rating and correspondingly high impact on the characteristics of a power system. Thus, multiple studies of VSM-based control strategies applied to HVDC transmission systems have recently been presented [8], [14]-[19]. These previous publications have mainly considered the operation of traditional 2-level (2L) Voltage Source Converters (VSCs), even if the Modular Multilevel Converter introduced in [20] is becoming the preferred topology for VSC HVDC transmission schemes. The first examples of studying the utilization of MMC-based HVDC terminals for providing virtual inertia and frequency support have recently been published in [21], [22], based on numerical simulations.

In this paper, an implementation of the VSM concept on a MMC is presented and demonstrated with a laboratory-scale setup. The experiments are based on an MMC prototype with 18 half-bridge sub-modules per arm. The VSM-based control system is relying on a virtual swing equation, a quasi-stationary virtual impedance and

This work was supported by the project "HVDC Inertia Provision" (HVDC Pro), financed by the ENERGIX program of RCN with project number 268053/E20 and the industry partners; Statnett, Statoil, RTE and ELIA.

Accpted for publication in:
2018 International Power Electronics Conference
DOI: 10.23919/IPEC.2018.8508009

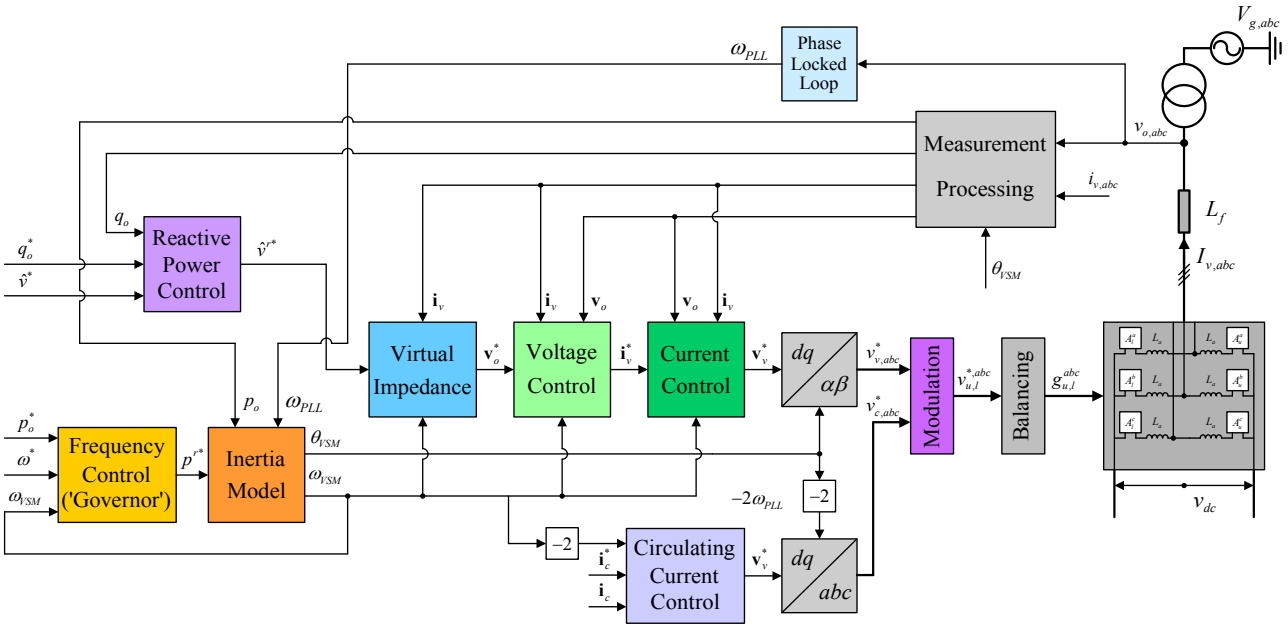

Fig. 1. Overview of VSM-based control system for a Modular Multilevel Converter

cascaded voltage and current controllers. Thus, the control of the ac-side of the MMC is derived from the VSM implementations presented in [7], [23]. The functionality of this VSM-based control scheme is integrated with the modulation strategy and the control of the circulating currents of the MMC. Experimental results demonstrate the intended operation and the expected dynamic performance in response to several external perturbations, both when connected to an external grid and when operated in islanded mode on a resistive load. Seamless transition between grid-connected and islanded mode following a sudden disconnection of the main grid is also demonstrated.

II. Control Strategy for an MMC Controlled as a Virtual Synchronous Machine

The control system implemented for the VSM-based operation of an MMC is outlined in this section. In the figures, upper case symbols indicate physical variables and parameters, while lower case symbols represent per unit quantities. Furthermore, bold symbols represent synchronous reference frame *dq* variables expressed as complex space vectors, i.e. as $\mathbf{x} = x_d + j\,x_q$.

A. VSM Control System Overview and Adaptations for Operation with an MMC

An overview of the implemented VSM-based control strategy for the MMC is shown in Fig. 1. For interpreting the structure of the control system, it should be considered that the MMC is controlled by two parallel control paths that are generating voltage references for driving the ac-side and circulating currents $i_{v,abc}$ and $i_{c,abc}$, respectively. Thus, the MMC has two independent sets of inner loop current controllers which are generating the ac-side and internal voltage references, v^*_v and v^*_c.

The individual modulation indices $n_{u,l}$ for controlling the upper (u) and lower (l) arms of each phase k of the MMC are calculated from the voltage references as:

$$n_{u,k} \approx \frac{-v^*_{v,k} + v^*_{c,k} + v_{dc}}{v_{dc}}, \quad n_{l,k} \approx \frac{v^*_{v,k} + v^*_{c,k} + v_{dc}}{v_{dc}} \qquad (1)$$
$$for \quad k \in \{a,b,c\}$$

This calculation of the arm insertion indexes implies that the equivalent gain of the control system is compensated for any variations in the available dc voltage. However, this modulation strategy does not compensate for the periodic oscillations appearing in the equivalent arm capacitor voltages. Indeed, if the actual or estimated arm voltages were used in the calculation of the insertion indices, it would be necessary to introduce closed loop control of the equivalent voltage or energy balance of the MMC [24]-[26].

In the presented implementation, the explicit energy control is avoided and the total equivalent voltages of each arm of the MMC will settle naturally to an operating point according to the power flow and the parameters of the MMC topology. Thus, only a Circulating Current Suppression Controller (CCSC), implemented as a set of decoupled PI controllers in the double frequency negative sequence synchronous reference frame according to [27], is introduced to regulate the internal circulating currents of the MMC. The CCSC is utilized for reducing the peak arm currents, the losses associated with the double frequency circulating currents and for limiting the corresponding internal oscillations of the MMC capacitor voltage. Thus, the current references for the circulating current controller indicated in Fig. 1 are set to (i.e. $\mathbf{i}^*_c = 0 + j\,0$) [27].

It can be noted that a sum energy controller investigated in [28] could also be easily introduced in the presented control scheme. This would decouple the total energy stored in the MMC from the voltage at the dc terminals, without requiring explicit control of the energy balance within the topology.

As shown by Fig. 1, the rest of the VSM-based control system relies on a set of cascaded voltage and current controllers, as well as a virtual impedance, for controlling the ac-side variables of the MMC. Furthermore, the control

Accpted for publication in:
2018 International Power Electronics Conference
DOI: 10.23919/IPEC.2018.8508009

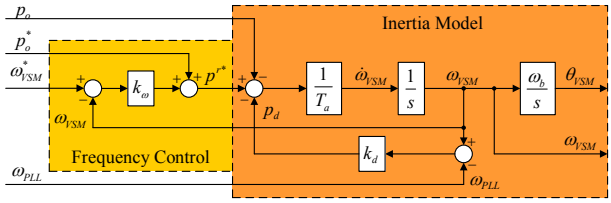

Fig. 2. Frequency droop control and the virtual swing equation implemented as the inertia model of the VSM

Fig. 3. Overview of laboratory setup and picture of circuit board with two half-bridge sub-modules

scheme includes a reactive power controller, the inertia model for emulating an SM swing equation, and a droop-based frequency control. These control functions can be almost identical to the VSM implementation presented in [7], [23] and are briefly summarized in the following.

B. Virtual Swing Equation and Frequency Control

The details of the inertia model and the frequency control from the lower left part of Fig. 1 are shown in Fig. 2 The implementation is based on [23], and, as seen from the figure, the emulated model includes the two main elements of the VSM, i.e. the inertia represented by the mechanical time constant *Ta*, and the mechanical damping power p_d. In this case, the damping of the swing equation is implemented by calculating the difference between the per unit speed of the virtual swing equation and the per unit grid frequency as detected by a PLL. Thus, under regular operation, the PLL in Fig. 1 does not have any other function than tracking the frequency, and is not involved in the grid synchronization of the control strategy.

Considering only the inertia emulation of the virtual swing equation in Fig. 2, the state equation of the virtual speed of the VSM can be defined by:

$$\frac{d\omega_{VSM}}{dt} = \frac{p^{r*}}{T_a} - \frac{p_o}{T_a} - \frac{k_d \cdot (\omega_{VSM} - \omega_{PLL})}{T_a} \tag{2}$$

However, the figure also shows that the input power reference to the inertia model, p^{r*}, is resulting from a simple power-frequency droop function according to:

$$p^{r*} = p_o^* + k_\omega \cdot (\omega_{VSM}^* - \omega_{VSM}) \tag{3}$$

From the control system overview in Fig. 1, it can be seen how the virtual per unit speed ω_{VSM} of the VSM and the phase angle θ_{VSM} are utilized in the control structure. It should be noted that the phase angle θ_{VSM}, resulting from integration of the virtual speed, is used for all *dq*-transformations in the system. Thus, the entire control system is implemented in synchronous reference frames defined by the virtual swing equation of the VSM.

TABLE I
MAIN PARAMETERS OF THE REDUCED-SCALE MMC PROTOTYPE

Converter parameters	Reference	18 HB model
Rated power	1059MVA	60 kVA
Rated DC voltage	640 kV DC	700V
Rated AC voltage|	333 kV	400V
Rated current	1836A	83A
Cells per arm	401 HB	18 HB
Nominal cell voltage	2 kV	50V
Arm inductance	50 mH	1,5 mH
Cell capacitance	10 mF	20 mF

C. Virtual Impedance

The structure of the outer loop reactive power droop control and cascaded voltage and current controllers shown in Fig. 1 can be identical for the MMC as for a 2L VSC. Thus, the implementation is based directly on [7], [23] and no further details are presented here. However, the virtual impedance emulating the voltage drop in the stator impedance of a SM has an important function since the current dependency of the voltage reference allows the cascaded voltage and current controllers to operate under strong grid conditions. For simplicity, a quasi-stationary implementation of this virtual impedance is preferred, and the resulting voltage reference is given by:

$$\mathbf{v}_o^* = \hat{v}^{r*} - \left(r_v + j \cdot \omega_{VSM} \cdot l_v\right) \cdot \mathbf{i}_o \tag{4}$$

III. HARDWARE IMPLEMENTATION OF MMC CONTROLLED AS A VSM

The VSM-based control system described in the previous section has been implemented on a reduced scale MMC prototype and tested in a laboratory environment with controllable ac- and dc-side voltage sources. This section provides a brief description of the hardware prototype and on the experimental setup.

A. Laboratory Scale MMC Prototype

The MMC converter prototype used in the experiments is a scaled-down version of a terminal from the HVDC transmission scheme described in [29]. The main specifications are reported in Table I. A picture with an overview of the laboratory setup and an image of the hardware for the sub-modules is shown in Fig. 3.

The control implementation for the MMC has a hierarchical and modular structure, as shown in Fig. 4. The system controller is located on the Opal-RT unit and is programmed in Simulink. It executes the VSM control and all the control loops of the MMC presented in the previous section, including the energy balancing and circulating current control. Outputs of the system controller are the six reference values for the converter arm voltages according to (1), which are sent to three individual leg controllers via a dedicated high-speed, full-duplex optical bus, operating at 5 Mbit/s. On the same bus, the leg controllers send back to the system controllers the measurements of the arm currents and the sum of the cell voltages in each arm, along with other monitoring information.

Accpted for publication in:
2018 International Power Electronics Conference
DOI: 10.23919/IPEC.2018.8508009

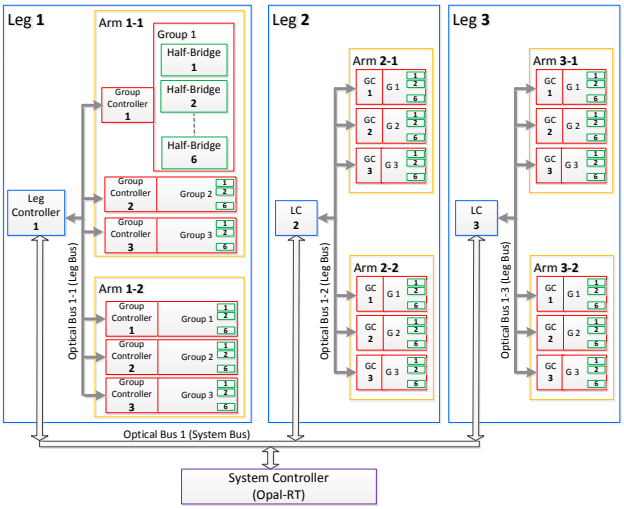

Fig. 4. MMC control and communication structure

Each leg controller is responsible for the balancing of the dc-voltages of the cells within the connected arms. Information about the individual cell voltages is collected through a dedicated optical bus, operating at 3.5 Mbit/s, connecting the leg controller to all the group controllers of the leg. The group controllers are directly connected to the half-bridge switching cells and are responsible for translating the voltage commands for each cell received from the leg controller into suitable gate signals for the switching devices. Strict synchronization of all the switching cells is achieved by the custom-made time-triggered protocol implemented on the optical buses.

B. System Configuration

The system configuration for the experimental tests is shown in Fig. 5. The MMC is connected on both the ac side and the dc side to individual outputs of a grid emulator controlled in real time by the OPAL-RT platform. The grid emulator is rated for 200 kW in total, and provides the possibility to independently control six individual output terminals with a voltage control bandwidth up to 20 kHz. Three of the outputs have been grouped together to form a controlled ac grid at 380 V LL RMS, while two other outputs have been grouped to act as a dc voltage source at 690 V. An adjustable resistive load is also placed on the ac bus, acting as local load when the switch connecting the emulated ac bus to the rest of the system is open, resulting in islanded operation of the VSM-controlled MMC. A transformer with unity voltage ratio is connected between the MMC output and the rest of the ac bus to ensure galvanic insulation.

As shown in Fig. 4, the Opal-RT real time simulator controls the grid emulator by providing adjustable reference signals for the voltage amplitude and frequency. References for the grid emulator and the MMC are transferred via two different 5 Mbit/s optical buses.

The presented configuration offers a high degree of flexibility for testing the effect of changes of references or control parameters in the converter as well as the effect of external transients in the ac and dc grid by acting on the references for the grid emulator. Moreover, the possibility to disconnect the emulated ac grid from the rest of the ac bus allows for testing the response of the VSM-controlled MMC in case of sudden islanding.

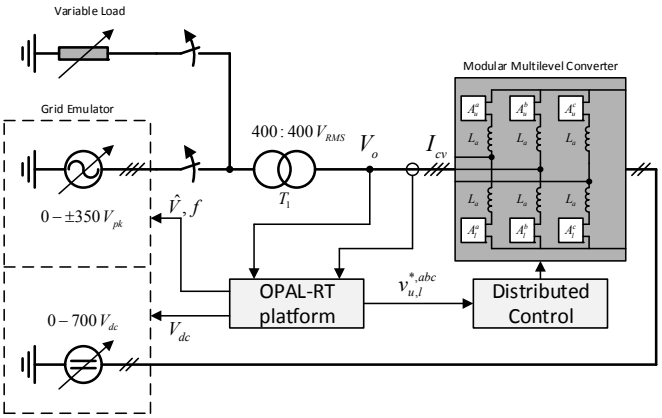

Fig. 5. System configuration for testing of MMC-based VSM

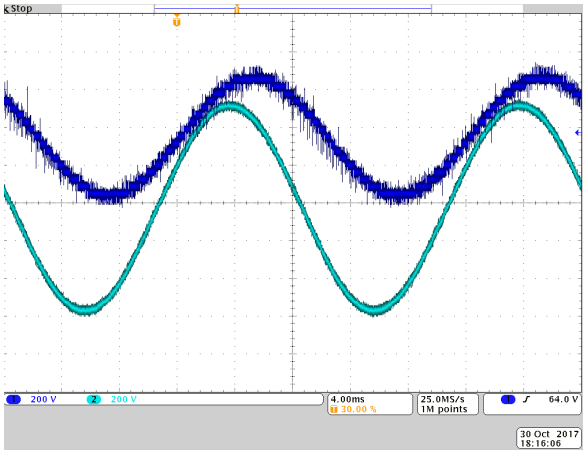

Fig. 6. MMC converter waveforms: Lower arm voltage of phase a and line-to-line voltage at output terminals

IV. Experimental Results

This section presents an experimental validation of the VSM functionalities both in grid connected operation and in islanded mode. Moreover, the smooth transition between grid connected and islanded operation that characterizes the VSM is demonstrated.

For all the experiments, the VSM control has been configured with an equivalent inertia constant T_a equal to 2 s, a droop gain k_ω of 20 and a damping factor k_d of 200.

The oscilloscope screenshot in Fig. 6 shows the lower arm voltage of phase *a* measured before the filter and referred to the negative dc rail; the voltage waveform features 19 different levels, consistently with the number of cells per arm of the converter. The line-to-line voltage between phase *a* and *b* at the output terminals of the MMC after the arm inductors is also shown, clearly demonstrating the low harmonic distortion achieved even with the basic filter constituted by the arm inductors only.

A. Grid connected operation

The VSM is operated while connected to an emulated 50 Hz, 380V ac grid. The system is initially in steady state with active power reference to the MMC set to 20 kW, reactive power reference set to zero and internal VSM voltage setpoint equal to 380V.

Accpted for publication in:
2018 International Power Electronics Conference
DOI: 10.23919/IPEC.2018.8508009

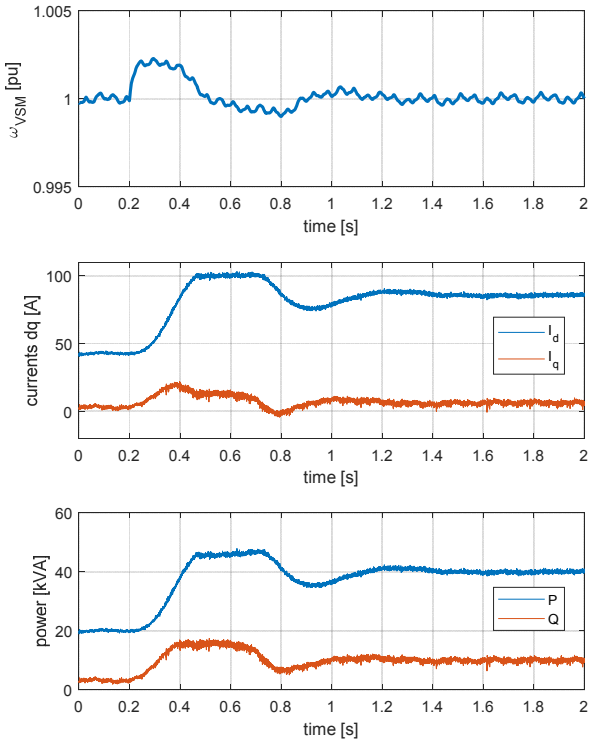

Fig. 7. Experimental results: VSM response to a step in power reference at nominal grid frequency

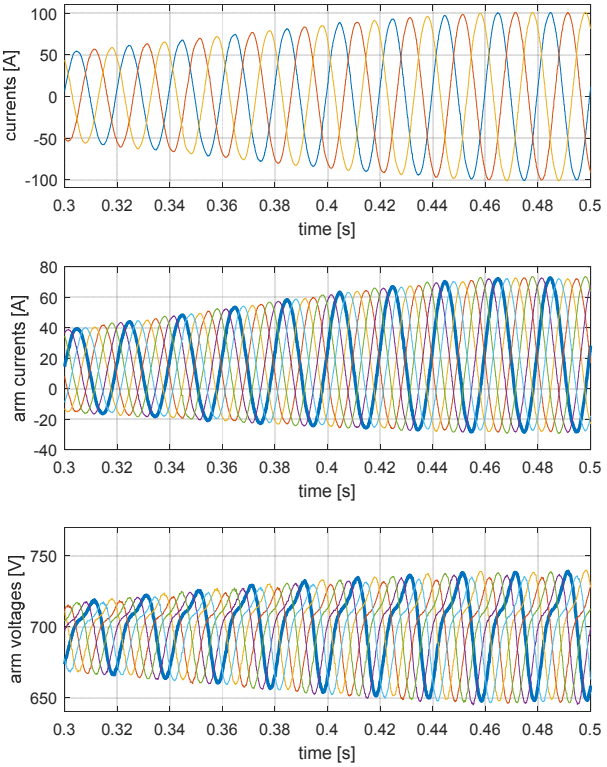

Fig. 8. Experimental results: VSM-MMC response to a step in power reference at nominal grid frequency. MMC output currents (top), arm currents (middle), arm voltages (bottom).

As a first test of dynamic response, the transient behavior of the system has been verified for a step change in the active power reference of the VSM from 20 kW to 40 kW, with key results plotted in Fig. 7. Since the grid emulator is maintaining the ac frequency at 50 Hz, the effect of the change in the active power reference directly translates into the same change in the power injected from the VSM to the grid. This is highlighted in the experimental results where the rotating speed of the VSM starts at 1.0 pu and returns to 1.0 pu after a damped transient as expected from the dynamics of the swing equation. The measured power displays a similar behavior with a damped second order transient before reaching the new steady state conditions. It should be noticed that the unlimited response of the VSM in this case would have presented an overshoot in the power and in the current. However, a current saturation set at 100 A limits the peak current during the transient, actively protecting the solid-state devices in the converter. Indeed, the ability to precisely control the currents during transients without altering the functional behavior of the VSM is a main feature of the proposed VSM implementation scheme.

The converter output currents in the stationary frame, together with the MMC arm voltages and currents are displayed in Fig. 8. Notably, arm voltages and currents remain well balanced throughout the transient, indicating that the VSM control is not interfering with the inner MMC control.

In the second test, the references of the VSM are maintained unaltered but the grid emulator is controlled to impose a step change in the frequency from 50 Hz to 49.8 Hz. The experiment aims at validating the inertia support offered by the VSM scheme and the effect of the droop in steady state. As shown by the results in Fig. 9, the VSM responds to a step decrease in the frequency as a synchronous generator, by a transient injection of power that in this case reaches a peak of approximately 35 kW. The active power and the virtual speed of the VSM settle to a new steady state condition after a brief oscillatory transient. The final steady state power is different from the initial operation, due to the presence of a droop characteristic in the VSM control. Indeed, the grid emulator imposes the frequency to a lower value, thus forcing the power injected from the VSM to a slightly higher value. This illustrates the double support contribution of the VSM to the receiving grid: a transient support action due to the response of the virtual inertia with an almost immediate power injection and a permanent support at steady state with an injection of power according to the droop characteristic. It should also be noticed that the VSM scheme offers the possibility to fine-tune these two contributions by acting individually on the inertia or the droop constant.

The response of the VSM to a change in the voltage amplitude of the grid voltage from 380 V to 345V is shown in Fig. 10. The transient indicates that the effect of the change on the active current component and on the VSM speed is relatively minor. However, due to the presence of a virtual impedance, the VSM reacts to the lowering grid voltage with an increased reactive current injection.

B. Transition from grid-connected to islanded operation

A main feature of the VSM is the capability of allowing for smooth and seamless transition from grid connected to islanded mode.

Fig. 11 shows the transient behavior of the system when the grid emulator is suddenly disconnected from the ac bus.

Accpted for publication in:
2018 International Power Electronics Conference
DOI: 10.23919/IPEC.2018.8508009

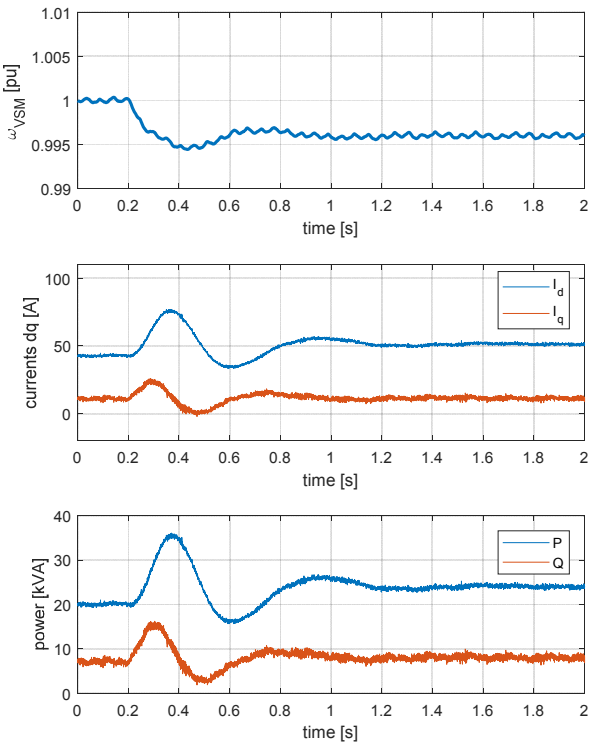

Fig. 9. Experimental results: VSM response to a step in the grid frequency

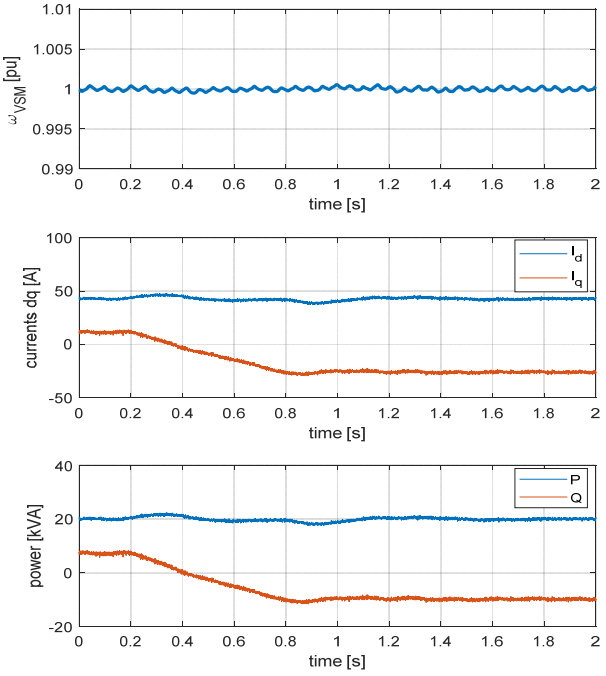

Fig. 10. Experimental results: VSM response to a variation in the grid voltage

The grid voltage feeding the local resistive load is controlled properly, with the voltage magnitude dropping less than 8% immediately after the islanding event and quickly recovering with a well-damped oscillation lasting for less than 300 ms. The transient on the grid frequency is properly damped by the virtual inertia, with oscillations extinguishing in a few seconds. The MMC operation is not disrupted by the islanding event, with arm voltages and

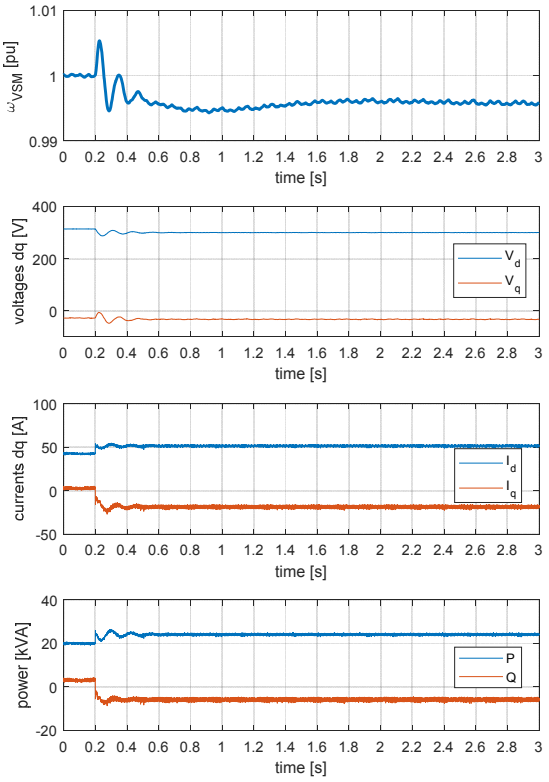

Fig. 11. Experimental results: VSM response to an islanding event

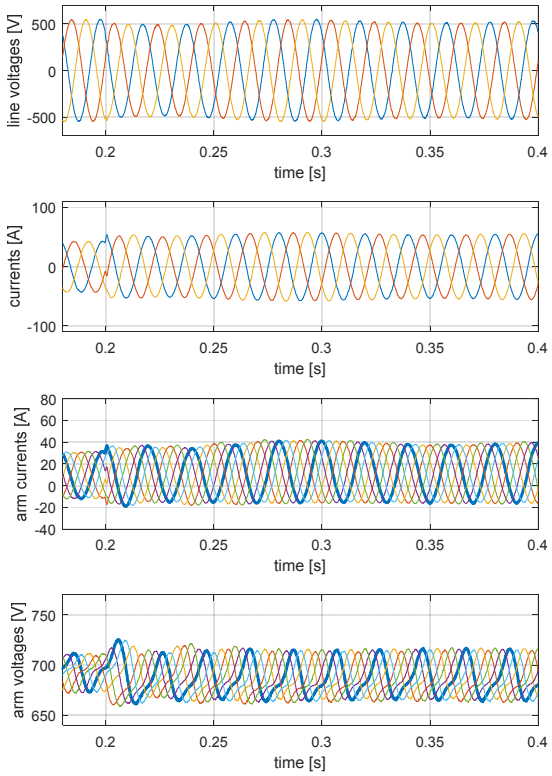

Fig. 12. Experimental results: VSM-MMC response to an islanding event; grid voltages and currents in stationary frame (top two graphs) and MMC arm currents and voltages (bottom two graphs)

currents remaining balanced and well under control throughout the transient, as shown in Fig. 12.

C. Islanded operation

As a last test the VSM is operated in islanded mode feeding a resistive load. The VSM is entirely responsible

Accpted for publication in:
2018 International Power Electronics Conference
DOI: 10.23919/IPEC.2018.8508009

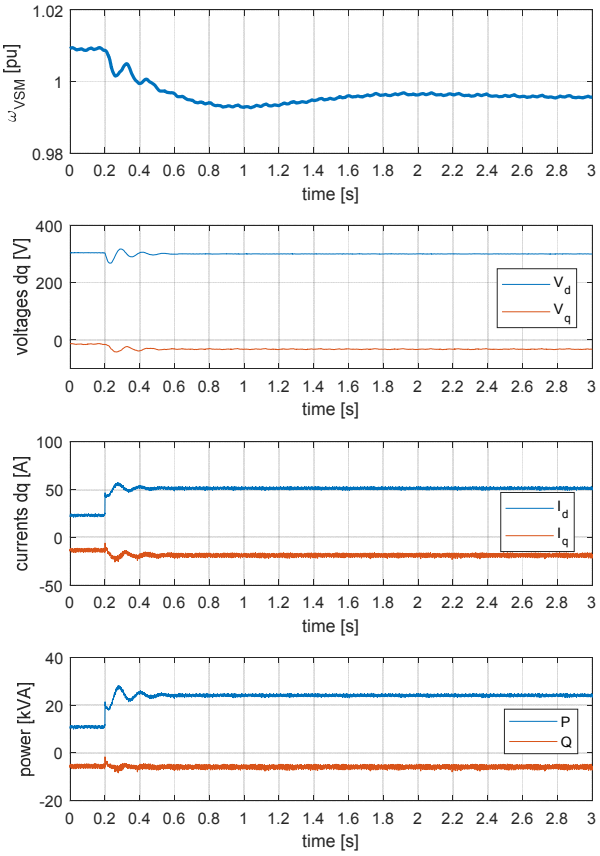

Fig. 13. Experimental results: VSM response to a load step while operating in islanded mode

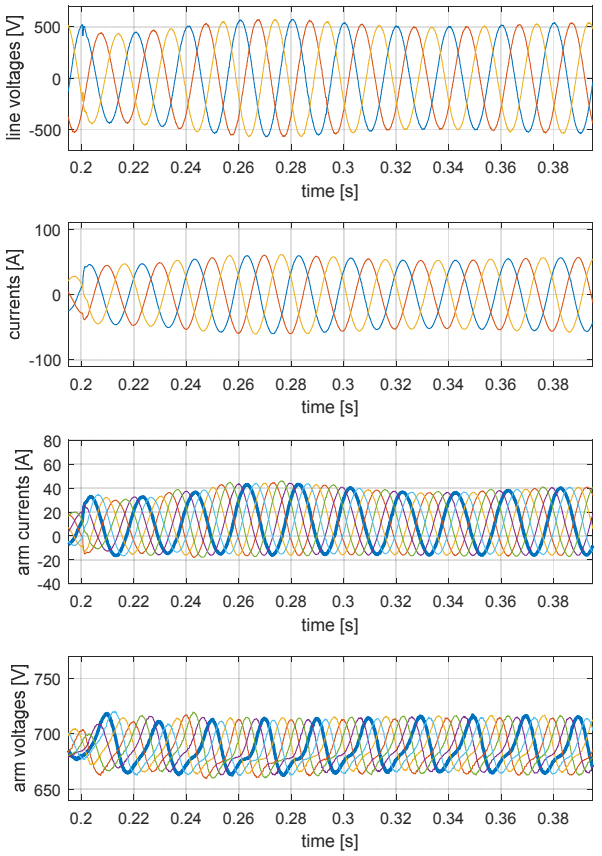

Fig. 14. Experimental results: VSM-MMC response to a load step while operating in islanded mode; grid voltages and currents in stationary frame (top two graphs) and MMC arm currents and voltages (bottom two graphs)

for the control of both voltage amplitude and frequency of the local grid. The effect of a step change in the load resistance from 11 Ohm to 5 Ohm is investigated.

Results in Fig. 13 show that the voltage regulation achieved by the VSM-controlled MMC is excellent, with hardly any dip observed in the grid voltage measured at the converter output terminals at t = 0.2 s, when the load is changed stepwise. The load step triggers small, well-damped oscillations with dynamics that are very similar to those observed after an islanding event.

The transient on the grid frequency, which in the islanded case coincides with the speed of the VSM, is also well damped, with the frequency settling to a lower value after the load is increased, as dictated by the droop coefficient in (3).

Robustness of the inner MMC control against grid disturbances is demonstrated by the results in Fig. 14, showing that arm currents and voltages remain balanced throughout the transient.

V. Conclusion

Inertia support from power converters is assumed to become a critical element in future power systems where the presence of physical rotating inertia is expected to be gradually reduced. The concept of Virtual Synchronous Machines offer a convenient approach to integrate inertia support functionality in the control of power converters together with the possibility to seamlessly switch between grid-connected and islanded operation. This control approach has initially emerged in the context of distributed generation systems, but can also be implemented in HVDC transmission schemes for supporting the frequency regulation of the power system. This paper presented an implementation of a Virtual Synchronous Machine scheme for the control of a MMC and its experimental validation. Several tests have been performed on a reduced-scale, MMC prototype controlled as a VSM, demonstrating its performance both when connected to an external ac grid or when operating in islanded mode. It has been shown that the proposed VSM implementation can operate without interfering with the internal operation of the MMC converter itself, thus allowing a direct migration of the algorithms developed for conventional 2-level converters to the more complex multilevel converters used in state-of-the-art HVDC systems.

VI. References

[1] H.-P. Beck, R. Hesse, "Virtual Synchronous Machine," in Proceedings of the 9th International Conference on Electrical Power Quality and Utilisation, Barcelona, Spain, 9-11 October 2007, 6 pp.

[2] K. Visscher, S. W. H. De Haan, "Virtual Synchronous Machines (VSG's) for Frequency Stabilization in Future Grids with a Significant Share of Decentralized Generation," in CIRED seminar 2008: Smart Grids for Distribution, Frankfurt, Germany, 23-24 June 2008, 4 pp.

[3] S. D'Arco, J. A. Suul, "Virtual Synchronous Machines – Classification of Implementations and Analysis of Equivalence to Droop Controllers for Microgrids," in Proceedings of IEEE PowerTech Grenoble 2013, Grenoble, France, 16-20 June 2013, 7 pp.

Accpted for publication in:
2018 International Power Electronics Conference
DOI: 10.23919/IPEC.2018.8508009

[4] S. D'Arco, J. A. Suul, O. B. Fosso, "Small-signal modelling and parametric sensitivity of a Virtual Synchronous Machine in islanded operation," in *International Journal of Electric Power and Energy Systems*, Vol. 72, November 2015, pp. 3-15

[5] Q.-C. Zhong, G. Weiss, "Synchronverters: Inverters That Mimic Synchronous Generators," IEEE Trans. on Ind. Electronics, vol. 58, no. 4, pp. 1259-1267, April 2011

[6] P. Rodriguez, I. Candela, A. Luna, "Control of PV Generation Systems using the Synchronous Power Controller," in Proc. of the 2013 IEEE Energy Conversion Congress and Exposition, ECCE 2013, Denver, Colorado, USA, 15-19 September 2013, pp. 993-998

[7] S. D'Arco, J. A. Suul, "Small-Signal Analysis of an Isolated Power System controlled by a Virtual Synchronous Machine," in *Proceedings of the IEEE 17th International Conference on Power Electronics and Motion Control*, PEMC 2016, Varna, Bulgaria, 25-30 September 2016, pp. 462-469

[8] E. Rakhshani, P. Rodriguez, "Inertia Emulation in AC/DC Interconnected Power Systems Using Derivative Technique Considering Frequency Measurement Effects," in IEEE Transactions on Power Systems, Vol. 32, No. 5, September 2017, pp.3338-3351

[9] D. Duckwitz, B. Fisher, "Modeling and Design of df/dt-based Inertia Control for Power Converters," in IEEE Journal of Emerging and Selected Topics in Power Electronics, Vol. 5, No. 4, December 2017, pp.1553-1564

[10] R. Hesse, D. Turschner, H.-P. Beck, "Micro grid stabilization using the Virtual Synchronous Machine (VISMA)," in *Proceedings of the International Conference on Renewable Energies and Power Quality*, ICREPQ'09, Valencia, Spain, 15-17 April 2009, 6 pp.

[11] Y. Chen, R. Hesse, D. Turschner, H.-P. Beck, "Investigation of the Virtual Synchronous Machine in the Island Mode," in *Proceedings of the 2012 3rd IEEE Innovative Smart Grid Technologies Europe Conference*, Berlin, Germany, 15-17 October 2012, 6 pp.

[12] T. Ackerman, T. Prevost, V. Vittal, A. J. Roscoe, J. Matevosvan, N. Miller, "Paving the Way: A Future Without Inertia Is Closer Than You Think," in IEEE Power and Energy Magazine, Vol. 15, No. 6, November/December 2017, pp. 61-.69

[13] Y. Wang, V. Silva, M. Lopez-Botet-Zulueta, "Impact of high penetration of variable renewable generation on frequency dynamics in the continental Europe interconnected system," in IET Renewable Power Generation, Vol. 10, No. 1, January 2016, pp. 10-16

[14] J. Zhou, C. Booth, G. P. Adam, A. J. Roscoe, "Inertia Emulation Control of VSC-HVDC Transmission System," in Proceedings of the 2011 International Conference on Advanced Power System Automation and Protection, Beijing, China, 16-20 October 2011, 6 pp.

[15] J. Zhu, C. D. Booth, G. P. Adam, A. J. Roscoe, C. G. Bright, "Inertia Emulation Control Strategy for VSC-HVDC Transmission Systems" in IEEE Transactions on Power Systems, Vol. 28, No. 2, May 2013, pp. 1277-1287

[16] R. Aouini, B. Marinescu, K. B. Kilani, M. Elleuch, "Synchronverter-Based Emulation and Control of HVDC Transmission," in IEEE Transactions on Power Systems, Vol. 31, No. 1, January 2016, pp. 278-286

[17] M. Guan, W. Pan, J. Zhang, Q. Hao, J. Cheng, X. Zheng, "Synchronous Generator Emulation Control Strategy for Voltage Source Converter (VSC) Stations," in IEEE Transactions on Power Systems, Vol. 30, No. 6, November 2016, pp. 3093-3101

[18] W. Zhang, K. Rouzbehi, J. I. Candela, A. Luna, P. Rodriguez, "Control of VSC-HVDC with Electromechanical Characteristics and Unified Primary Strategy," in Proc. of the 2016 IEEE Energy Conversion Congress and Exposition, ECCE 2016, Milwaukee, Wisconsin, USA, 18-22 September 2016, 8 pp.

[19] E. Rakshani, D. Remon, A. M. Cantarellas, J. M. Garcia, P. Rodriguez, "Modeling and sensitivity analysis of VSP based virtual inertia controller in HVDC links of interconnected power systems," in Electric Power System Research, Vol. 141, Dec. 2016, pp. 246-263

[20] A. Lesnicar, R. Marquardt, "An innovative modular multilevel converter topology suitable for a wide power range, in Proceedings of the 2003 IEEE Bologna PowerTech Conference, Bologna, Italy, 23-26 June 2003, vol.3, pp. 272-277

[21] C. Verdugo, J. I. Candela, P. Rodriguez, "Grid Support Functionalities based on Modular Multilevel Converters with Synchronous Power Control," in Proceedings of the 5th International Conference on Renewable Energy Research and Applications, Birmingham, UK, 20-23 November 2016, pp. 572-577

[22] O. D. Adeuyi, M. Cheah-Mane, J. Liang, N. Jenkins, Y. Wu, Z. Li, X. Wu, "Frequency Support from Modular Multilevel Converter Based Multi-Terminal HVDC Schemes," in Proc. of the 2015 IEEE Power and Energy Society General Meeting, PESGM 2015, Denver, Colorado, USA, 26-30 July 2016, 5 pp.

[23] S. D'Arco, J. A. Suul, O. B. Fosso, "Small-Signal Modeling and Parametric Sensitivity of a Virtual Synchronous Machine," in *Proceedings of the 18th Power Systems Computation Conference*, PSCC 2014, Wrocław, Poland, 18-22 August 2014, 9 pp.

[24] A. Antonopoulos, L. Ängquist, H.-P. Nee, "On Dynamics and Voltage Control of the Modular Multilevel Converter," in *Proceedings of the 13th European Conference on Power Electronics and Applications*, EPE'09, Barcelona, Spain, 8-10 September 2009, 10 pp

[25] L. Harnefors, A. Antonopoulos, S. Norrga, L. Ängquist, H.-P Nee, "Dynamic Analysis of Modular Multilevel Converters," in *IEEE Transactions on Industrial Electronics*, vol. 60, no. 7, July 2013, pp. 2526-2537

[26] G. Bergna J. A. Suul, S. D'Arco, "State-Space Modeling of Modular Multilevel Converters for Constant Variables in Steady-State," in *Proceedings of the 17th IEEE Workshop on Control and Modeling for Power Electronics*, COMPEL 2016, Trondheim, Norway, 27-30 June 2016, 9 pp.

[27] Q. Tu, Z. Xu, L. Xu, "Reduced Switching-Frequency Modulation and Circulating Current Suppression for Modular Multilevel Converters," in *IEEE Transactions on Power Delivery*, Vol.26, No.3, pp.2009-2017, July 2011

[28] J. Freytes, G. Bergna, J. A. Suul, S. D'Arco, F. Gruson, F. Colas, H. Saad, X. Guillaud, "Improving Small-Signal Stability of an MMC with CCSC by Control of the Internally Stored Energy," in *IEEE Transactions on Power Delivery*, Vol. 33, No. 1, February 2018, pp. 429-439

[29] J. Peralta, H. Saad, S. Dennetiére, J. Mahseredjian and S. Nguefeu, "Detailed and Averaged Models for a 401-Level MMC-HVDC System," in IEEE Transactions on Power Delivery, vol. 27, No. 3, pp.1501-1508, July 2012